Heliyon 10 (2024) e26631

Contents lists available at ScienceDirect

Heliyon

journal homepage: www.cell.com/heliyon

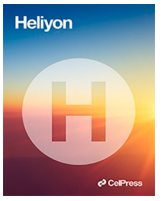

Research article

Hydrothermal synthesis of NiO nanoparticles decorated hierarchical MnO_2 nanowire for supercapacitor electrode with improved electrochemical performance

Muhammad Rakibul Islam [a,*], Mahabub Alam Bhuiyan [b], Md Hasive Ahmed [a], Mizanur Rahaman [a]

[a] Department of Physics, Bangladesh University of Engineering and Technology, Dhaka, Bangladesh
[b] Department of Physics, University of Dhaka, Dhaka, Bangladesh

ARTICLE INFO

Keywords:
MnO_2 nanowire
NiO nanoparticle
Electrochemical properties
Specific capacitance

ABSTRACT

In this work, MnO_2/NiO nanocomposite electrode materials have been synthesized by a cost-effective hydrothermal method. The effect of the concentrations (0, 1, 3, 5, and 7 wt%) of NiO nanoparticles on the surface morphology, structural properties, and electrochemical performance of the nanocomposites was characterized by different characterization techniques. The scanning electron micrographs (SEM) reveal that the as-prepared NiO nanoparticles are well connected and stuck with the MnO_2 nanowires. The transmission electron microscopy (TEM) analysis showed an increase in the interplanar spacing due to the incorporation of NiO nanoparticles. The different structural parameters of MnO_2/NiO nanocomposites were also found to vary with the concentration of NiO. The MnO_2/NiO nanocomposites provide an improved electrochemical performance together with a specific capacitance as high as 343 F/g at 1.25 A/g current density. The electrochemical spectroscopic analysis revealed a reduction in charge transfer resistance due to the introduction of NiO, indicating a rapid carrier transportation between the materials interface. The improved electrochemical performance of MnO_2/NiO can be attributed to good interfacial interaction, a large interlayer distance, and low charge transfer resistance. The unique features of MnO_2/NiO and the cost-effective hydrothermal method will open up a new route for the fabrication of a promising supercapacitor electrode.

1. Introduction

The record-setting world economic growth and human civilization over the past decades are coming at the expense of fossil fuels and environmental deterioration, which results from the emergence of the energy crisis [1,2]. The lack of alternative sustainable energy and their storage has become one of the major concerns of the world [3–5]. To resolve this global crisis, extensive research has been carried out, which has helped us to understand the underlying science of energy storage kinetics and has improved the energy storage in different kinds of devices such as fuel cells, batteries, solar cells, supercapacitors, and many other electrochemical devices [6–11]. Among these energy storage devices, supercapacitors have proven themselves a promising energy storage candidate due to their superior characteristics, such as higher power and energy density, excellent cycle performance, and faster charge/discharge

* Corresponding author.
E-mail address: rakibul@phy.buet.ac.bd (M.R. Islam).

https://doi.org/10.1016/j.heliyon.2024.e26631
Received 4 November 2023; Received in revised form 31 January 2024; Accepted 16 February 2024
Available online 17 February 2024
2405-8440/Â© 2024 The Authors. Published by Elsevier Ltd. This is an open access article under the CC BY-NC license (http://creativecommons.org/licenses/by-nc/4.0/).

efficiency compared to batteries and other energy storage devices [12–15]. Current research focuses on the synthesizing of innovative and highly efficacious nanostructured electrode materials with desired electrochemical properties since the efficiency of the supercapacitor relies highly on the dimensionality, geometry, and surface properties, chemical, mechanical, and thermal stabilities of the electrode materials [16–18]. Recently abundant and non-precious metal oxides such as Co_3O_4, Fe_3O_4, MnO_2, NiO, ZnO, and CuO nanostructures have attained great attention from many researchers as electrode materials due to their high porosity and large specific surface area [19–23]. Along with other factors, these two key components can provide superior specific capacitance and high energy density in these metal oxide electrode-based pseudocapacitors [24]. Concerning these, current research focuses on one-dimensional metal oxide nanostructures *e.g.,* nanotubes, nanofibers, nanorods, nanowires, etc., owing to their large active surface area [25]. Among those metal oxides, MnO_2 is considered one of the most attractive electrode materials due to its high theoretically predicted specific capacitance (~1370 F/g), abundance, low manufacturing cost, eco-friendly, diverse structures and oxidation states, thermal stability, and wide potential window and for its use in neutral electrolytes [26,27]. In the MnO_2 electrode, the intrinsic electronic conductivity and the diffusivity of the electrolyte cation into the lattice determine the pseudocapacitance of the electrode materials [26,28].

Despite the appealing characteristics/properties of pristine MnO_2, low electronic conductivity (10^{-5}-10^{-6} S cm^{-1}), larger diffusion paths, dissolution in aqueous electrolytes, and irreversible crystal volume expansion result in poor electrochemical response in terms of capacitance, cycling stability, and rate capability, which limits the practical application of pristine MnO_2 as an efficient electrode material [29–32].

To overcome these issues and improve the capacitive performance of MnO_2-based electrodes, numerous techniques have been developed. According to the literature, fabrication of MnO_2-based organic and inorganic nanocomposites is the common technique to elevate the capacitive performance of the MnO_2 electrodes [33–35]. Recently, metal oxide-incorporated MnO_2 nanocomposites have attracted much attention since they have demonstrated better collective pseudocapacitance contributions as well as cyclic stability [36,37]. Among them, nickel oxide (NiO) nanoparticles can be considered as one of the promising transition metal oxides for the suitable incorporation with MnO_2 nanostructures due to its high theoretically predicted specific capacitance (2584 F/g), thermal stability, low cost and availability, benign nature to the environment and impressive reversible redox reaction [38,39]. Even though the supercapacitive behavior of the individual NiO and MnO_2 nanostructured electrode materials have been studied thoroughly [28, 40,41], the capacitive performance of the integrated nanostructures by these two materials is still in its infancy. However, recently, it has gained some research interest, and according to the available reported literature, it is expected that this NiO-integrated MnO_2 hybrid nanocomposite can be the desired electrode for high-performance supercapacitors. For example, J. P. Liu et al. [42] and Y. H. Li et al. [43] fabricated NiO/MnO_2 hybrid nanostructures and hierarchical nanosheet matrices on steel and carbon fiber paper, respectively, which improved specific capacity. M. AlAnazi et al. [44] have investigated several physical properties of multilayered MnO (n)/NiO (p) heterojunction thin film for supercapacitor applications. This heterojunction increases electrical conductivity, reduces bandgap and raises overall carrier density. The specific capacitance of two and four alternative layers are 3.6×10^3 and 5.8×10^3 F g^{-1} and capacitance retention of 14.8 and 12.9%. X. Zhao et al. [45] developed MnO_2@NiO nanosheets@nanowires and used as binder-free electrodes. The MnO_2@NiO integrated structure exhibits capacitive performance 374.6 F g^{-1} at a current density of 0.25 Ag^{-1} with excellent cyclic stability. N. Zhang et al. [46] have synthesized porous flowers like MnO_2–NiO anode material for lithium-ion batteries. The nanostructured NiO inhibits the volume expansion of MnO_2 during cyclic charging and discharging and demonstrates specific capacitance 2981 mAh·g^{-1} at a current density of 100 mA g^{-1} that is much higher than pure MnO_2. M. Arunpandian et al. [47] reported rGO-decorated MnO_2@NiO nanohybrids reveal improved specific capacitance. Y. Bi et al. [48] found superior cyclic stability and specific capacitance retention of 140% for 1500 cycles in their microwave-synthesized NiO/MnO_2 nanocomposite electrodes. T.-F. Yi et al. [49] have prepared a 3D spherical core-shell NiO/MnO_2 structure on nickel foam and observed improved cycle performance and rate capability, attributed to the strong interfacial interaction between multi-components of the 3D structure. K. M. Racik et al. [50] found good electrochemical performance in their MnO_2/NiO electrodes while KOH is used as an electrolyte. M. Zhange et al. [51] reported high specific capacitance (529 F/g at 1 A/g) in their electrodeposited MnO_2 supercapacitor on 3D porous Ni foam. From this discussion, it is clear that the incorporation of NiO improves the electrochemical performance of MnO_2. For device applications, it is essential to know the optimized concentration of NiO that may provide the best performance. Therefore, it is necessary to understand the effect of the concentration of NiO on the electrochemical performance of MnO_2. In this article we aim to study the effect of the concentration of NiO nanoparticles on the electrochemical performance of MnO_2.

Designing hierarchical three-dimensional (3D) architectures and complex core-shell structures can offer a higher surface area but often experience interfacial contact resistance, affecting the charge transport kinetics [36,37]. Furthermore, the fabrication process of these hierarchical architectures and core-shell structures is relatively time-consuming and complicated but provides low yield. Therefore, it is desirable to fabricate MnO_2-based nanocomposites in a very simple and cost-effective way that can offer better electrochemical performance. Considering these, the synthesis of MnO_2 nanowires and the incorporation of NiO nanoparticles into it by a facile and low-cost hydrothermal process may address these issues. The incorporation of NiO nanoparticles may introduce structural defects along with more active sites for ion diffusion. Furthermore, two different kinds of oxides (MnO_2 and NiO) may create an energy barrier, providing a shorter diffusion path for the ions and electrons [52–54]. Consequently, fast redox reaction and enhanced rate capability from nanocomposite electrodes can be expected.

Here, we report the fabrication of MnO_2/NiO nanocomposite as advanced supercapacitor electrode materials via a simple hydrothermal method. We incorporated different concentrations of NiO nanoparticles onto the nanowires shape MnO_2 to prepare the composite structures. The effect of NiO concentration on various physical and electrochemical properties of the synthesized electrode materials has been investigated by a standard characterization approach and is summarized in this study. Our MnO_2/NiO nanocomposite electrode demonstrated improved electrochemical performance, which is attributed to the larger surface area, shorter

diffusion path for the ions and electrons, and enhanced conductivity. We believe that our nanocomposite materials prepared by the cost-effective method can be employed in supercapacitor applications and will enrich the current library of energy storage electrode materials.

2. Experimental section

2.1. Materials

With no further refinement, chemical reagents of analytical purity were used. Both Dimethyl sulfoxide (C_2H_6OS) and Manganese sulfate monohydrate ($MnSO_4.H_2O$) were obtained from Merck in Darmstadt, Germany. Thiourea (CH_4N_2S), Urea (CH_4N_2O), Polyvinyl alcohol (PVA) $(C_2H_4O)_x$, Sodium sulfate (Na_2SO_4), Nickel nitrate hexahydrate ($Ni(NO_3)_26H_2O$), Urea (CH_4N_2O) and Amonia water (NH_4OH) were collected from SRL and Research Lab in India, respectively.

2.2. Synthesis of MnO_2 nanowires

A certain amount of $MnSO_4.H_2O$ was added to 140 ml deionized (DI) water, and then a specific amount of $KMnO_4$ was to the previous solution. After 30 min of continuous stirring, the solution was put into a 200 mL Teflon tube autoclave and heated at 140 °C for 12 h. Afterward, the brown precipitate was centrifuged and repeatedly cleaned with ethanol and DI water. Finally, the resulting brown powder was calcined in a furnace for 3 h at 300 °C, yielding the MnO_2 nanowire.

2.3. Preparation of NiO nanoparticles

A similar synthesis method was employed to prepare NiO nanoparticles. At first, an appropriate amount of $Ni(NO_3)_26H_2O$ was dissolved into 50 ml distilled water under continuous magnetic stirring. At this time, the solution of CH_4N_2O dropwise was added to the previous solution and stirred for proper mixing. Afterward, NH4OH was added for maintain the PH level under 8, and then the solution was stirred for 30 min. Then, the solution was poured into a Teflon line stainless steel autoclave and kept at 180 °C for 24 h. After cooling down the autoclave to room temperature, the precipitate was collected by centrifuge and followed by a few times washing it with distilled water and ethanol. Then, the obtained product was dried overnight at 60 °C, and the powder calcined at 400 °C for 3 h to get NiO nanoparticles.

2.4. Fabrication of MnO_2/NiO nanocomposite

A facile hydrothermal synthesis technique was used to fabricate the MnO_2/NiO nanocomposite. For example, to synthesize 1 wt% NiO incorporated MnO_2 nanocomposite, an appropriate amount of prepared NiO nanoparticles was dispersed into 50 ml distilled water by bath sonication. In another beaker, 70 ml solution of $KMnO_4$ and $MnSO_4.H_2O$ were mixed and continued vigorous stirring for 30 min. When the solution became homogenous, the above NiO dispersion solution was added to it and followed by vigorous magnetic stirring for an hour. After that, the mixture was poured into a Teflon-lined autoclave and placed in an oven at 140 °C for 12 h, followed

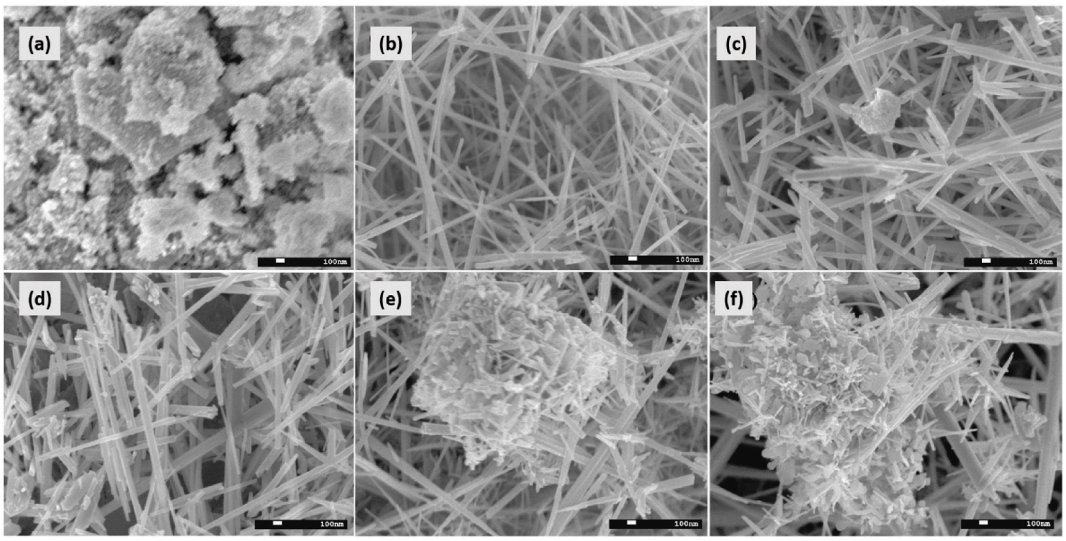

Fig. 1. FESEM image of (a) NiO nanoparticles, (b) MnO_2 nanowires, (c) MnO_2/NiO (1%), (d) MnO_2/NiO (3%), (e) MnO_2/NiO (5%), and (f) MnO_2/NiO (7%) nanocomposites.

by natural cooling down to room temperature. The obtained product was then centrifuged to collect the precipitate from the supernatant and washed several times with distilled water and ethanol. The collected washed clay was then dried at 60 °C for a few hours in an air oven to obtain the desired MnO_2/NiO nanocomposite. This prepared nanocomposite was termed MnO_2/NiO (1%) and a synthesis scheme of such composite materials is shown in Fig. 1. In this research work, different concentrations of NiO such as 1%, 3%, 5%, and 7% was fabricated and used for studies which are labeled as MnO_2/NiO (1%), MnO_2/NiO (3%), MnO_2/NiO (5%) and MnO_2/NiO (7%), respectively.

2.5. Electrode preparation

The working electrodes were fabricated using a method reported in our earlier work [5]. At first, a slurry mixture of active nanomaterials (70 mg) was prepared by mixing it with polyvinyl alcohol PVA (4 wt% of the active materials) and dimethyl sulfoxide (DMSO), where these two serve as the binder and solvent, respectively. In order to obtain a good slurry, the mixture was sonicated for around 60 min. Afterward, this slurry was deposited 0.4 mg on previously cleaned modified graphite electrodes by micropipette. Finally, the electrodes were dried at 60 °C for a few hours, and it served as the current collector in electrochemical measurements.

2.6. Characterizations

The surface morphology of the prepared MnO_2/NiO nanocomposites was investigated by a JSM 7600 field emission scanning electron microscope operated at an accelerating voltage of 5 kV, while the micromorphology of the synthesized electrode materials was assessed using a JEOL 2100F high-resolution transmission electron microscope (HR-TEM). For HR-TEM studies, a transparent holey carbon-coated standard copper grid was used. The crystal structure and different parameters of the synthesized MnO_2 nanowires and MnO_2/NiO composites were determined using CuK_α radiation ($\lambda = 1.5406$ Å) in a Philips 3040XPert Pro X-ray diffractometer. To probe the vibrational structure of the prepared materials, a red laser ($\lambda = 785$ nm) (HORIBA MacroRam) equipped with a CCD/InGaAs photodetector was employed to record the Raman spectra.

Electrochemical properties of the MnO_2 and MnO_2/NiO composites were examined using a CS310 electrochemical workstation (corrtest, china). A conventional three-electrode configuration was employed to perform the electrochemical measurements, where modified graphite was the working electrode, a 1 cm × 1 cm platinum plate was the counter electrode, and the reference electrode was silver/silver chloride (Ag/AgCl). The performance was measured using 0.5 M Na_2SO_4 aqueous solution as the neutral electrolyte.

3. Result and discussion

3.1. Scanning electron microscopy analysis

The surface morphology of the prepared samples was studied by scanning electron microscope (SEM), and the recorded SEM images for pristine NiO, MnO_2, and MnO_2/NiO composites are presented in Fig. 1(a–f). Fig. 1(a) depicts grown NiO nanoparticles (NPs), which are non-uniform in size, randomly oriented, and possess rough surfaces. These NPs are aggregated, leading to the

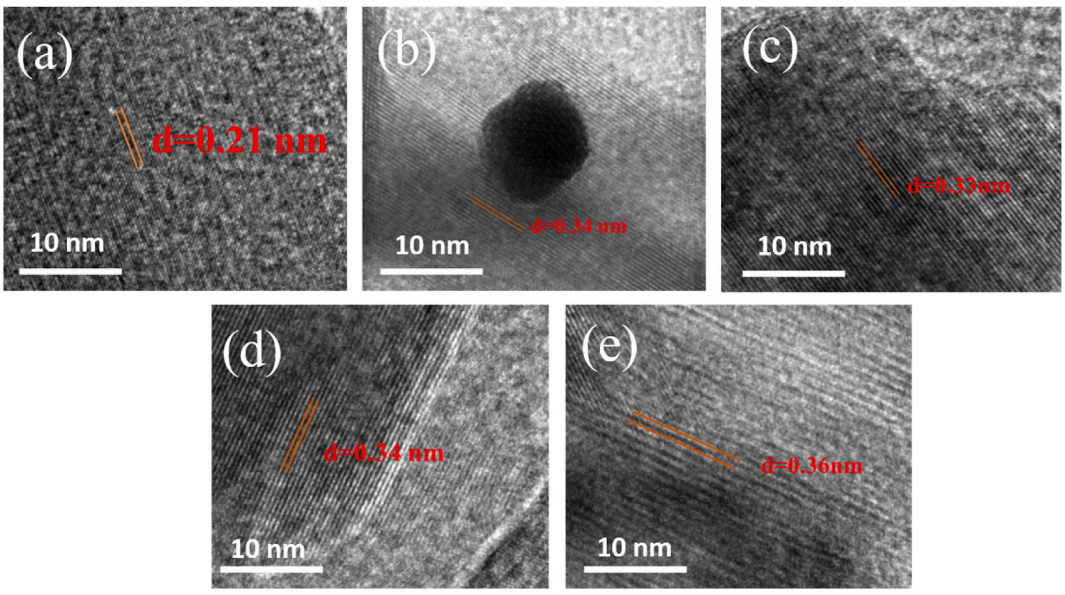

Fig. 2. HR-TEM image of (a) MnO_2, (b) MnO_2/NiO (1%), (c) MnO_2/NiO (3%), (d) MnO_2/NiO (5%), and (e) MnO_2/NiO (7%) nanocomposiotes.

formation of clusters, which are attributed to the nucleation centers available during the hydrothermal synthesis process [55]. Fig. 1(b) revealed that the as-prepared MnO_2 nanowire is very thin, having an average diameter of 40–50 nm and elongated up to several microns, therefore termed a nanowire (NWs). These nanowires are quite similar in size, transparent, and randomly oriented in different directions. Fig. 1(c–f) illustrates the SEM images for the increasing concentration of NiO in MnO_2 NWs. It is noticed that at low concentrations of incorporated NiO (1% and 3%), it is rarely stuck and covers a very tiny portion of MnO_2 NWs. Further increase in NiO incorporation started to cover a larger portion of MnO_2 NWs. The largest coverage is achieved for 7% NiO incorporation. In addition, with incease of the concentration of NiO nanoparticles, the porosity and pore size of all nanocomposites reduced. It is evident from Fig. 1(f) that although the NiO NPs are randomly oriented, they are well connected, stuck with the MnO_2 NWs, and distributed throughout the composite materials. Moreover, increasing the NiO concentration increases the irregularity in MnO_2 NWs and provides a rougher surface by sticking onto MnO_2 NWs. These features (enhanced irregularity, well interconnections of NiO clusters with MnO_2 NWs, enhanced rough surface) may provide higher porosity and larger surface area and thus can be expected to show improved electrochemical performance for this 7% NiO incorporated electrode material.

3.2. Transmission electron microscopy

To obtain further insights into the structure of the pristine and NiO-incorporated MnO_2 nanocomposite materials, high-resolution transmission electron microscopy (HR-TEM) studies were carried out and are presented in Fig. 2(a–e). From the HR-TEM image (Fig. 2 (a)) of pristine MnO_2 nanowires, the average interplanar spacing is found to be 0.21 nm, which is consistent with the (211) plane of MnO_2 nanowires [56]. For the incorporation of 1%, 3%, 5%, and 7% NiO nanoparticles into MnO_2, the d-spacing was obtained as 0.34, 0.33, 0.34, and 0.36 nm, respectively. Thus, increasing the doping concentration of NiO increases the interplanar spacing in the MnO_2 nanostructures. This increase in d-spacing is owing to the lattice mismatch and the creation of defects in the MnO_2 host lattice by the NiO nanoparticles.

3.3. X-ray diffraction

The crystal structure of the prepared electrode materials was analyzed by XRD. Fig. 3 illustrates the XRD pattern of the studied materials. The diffraction peaks for pristine MnO_2 nanowires at 2θ values 12.8°, 18.4°, 28.6°, 37.7°, 49.5°, 60.6°, and 69.8° which correspond to (110), (200), (310), (211), (301), (411), (521), (541) planes of the tetragonal structure ($a = b = 0.979$ nm and $c = 0.328$ nm) of MnO_2 crystal (JCPDS card number 24–0735). The narrow (211) peak confirms the good crystallinity of synthesized pristine MnO_2 NWs. No characteristic diffraction peaks of NiO have been detected in the XRD pattern of the composite materials. This may be due to the low concentration of the incorporated NiO in the MnO_2 crystal. However, the main reflection plane, *i.e.* (211) peak intensity, decreases as well as broadened with the increasing NiO concentration, owing to the poor crystallization due to lattice mismatch and defects. Furthermore, the (211) peak is shifted to the higher 2θ values for the increasing concentration of incorporated NiO, which suggests the contraction of lattice cell volume. It might seem unusual that a dopant (Ni^{2+}) with a larger ionic radius (0.7 nm) than the ionic radius of Mn^{4+} (0.67 nm) decreased the lattice parameters and cell volume. However, a theoretical study by Duan et al. conducted on Fe^{3+} (0.69 nm) doping into MnO_2 illustrated the contraction of cell volume due to the reduction of average M − O bond length [57]. M. Lube et al. experimentally observed a similar reduced cell volume when MnO_2 was incorporated with (Ni^{2+}) [58].

The (211) reflection peak has been used to determine the average crystalline size (L) by using Debye-Scherrer's formula [59],

$$L = \frac{0.94\lambda}{\beta \cos\theta}.$$

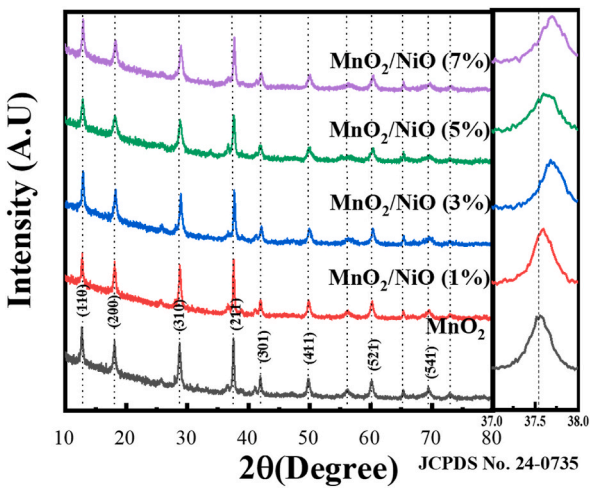

Fig. 3. XRD patterns of MnO_2 nanowire and MnO_2/NiO nanocomposites.

Here, λ is the wavelength of the used X-ray, β is the full width at half maximum, and θ is the diffraction angle at the highest intensity peak. The determined crystallite size (L) was further used to calculate the dislocation density [60],

$$\delta = \frac{1}{L^2}.$$

Also, the microstrain (ε) and lattice constants ($a, b,$ and c) of the MnO_2/NiO composites were determined by the following formulae respectively [60,61],

$$\varepsilon = \frac{\beta}{4\ tan\ \theta}$$

$$\frac{1}{d^2} = \frac{h^2 + k^2}{a^2} + \frac{l^2}{c^2}.$$

Here, d is the interplanar spacing, and (hkl) is the Miller indices. Fig. 4 represents the calculated structural parameters of all nanocomposites. Fig. 4 shows that the atomic spacing, lattice constants, and nanocrystal size are reduced with increasing NiO concentration. We expect that the reduction of these parameters may enhance the active site and material efficiency. A reduction in the crystallite size also suggest an increase of surface area due to the incorporation of NiO nanoparticles. Furthermore, this may limit the volume and expansion during the charging/discharging process, which might result in good cyclic stability of the MnO_2/NiO (7%) composite.

3.4. Raman analysis

Structural defects and local distortion in our synthesized composite materials were probed by Raman spectroscopy and are presented in Fig. 5. For MnO_2-based nanomaterials, theoretically, it is expected to observe a total 15 spectroscopic modes ($6A_g$, $6B_g$, and $3E_g$). However, in the polycrystalline MnO_2 sample, some of these modes are poorly polarizable, and a few of them are incompletely resolved overlapped modes, which hinders the observation of the above 15 Raman modes [62]. Here, in our prepared pristine MnO_2 materials, two sharp peaks at about 574 and 634 cm^{-1} and three weak bands at 295, 346, and 494 cm^{-1} have been recorded (Fig. 5). In this Raman spectroscopy, three Raman bands at 346, 574 and 634 cm^{-1} are assigned to A_g symmetry. In particular, 346, 574, and 634 cm^{-1} correspond to the stretching vibration of Mn–O in the basal plane of the MnO_6 group, the vibration of the O–Mn–O–Mn chains in the octahedral planes, and the symmetric vibration stretching of O–Mn–O perpendicular to the direction of the octahedral double

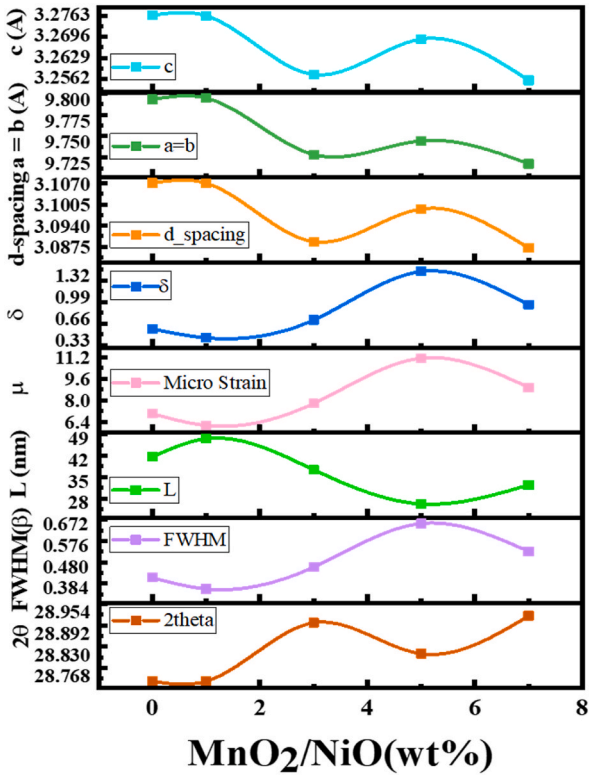

Fig. 4. Effect of various concentration of NiO nanoparticles on the structural parameters of MnO_2/NiO nanocomposites.

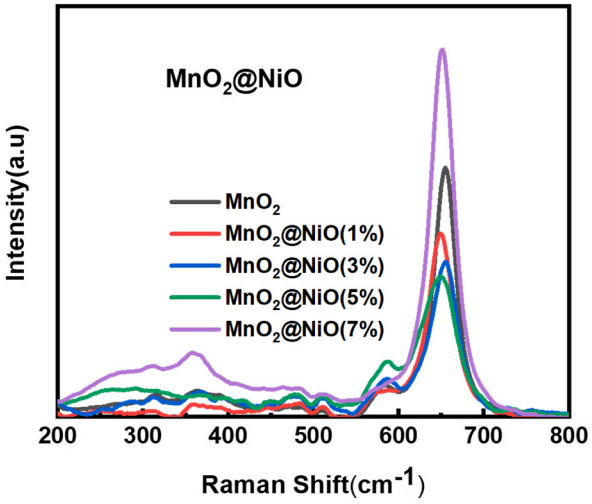

Fig. 5. Raman spectra of MnO_2 and MnO_2/NiO nanocomposites.

chains of MnO_2, respectively [62,63]. Here, it is worth mentioning that in MnO_2, Raman peaks are the collective vibration mode of octahedron MnO_6 [64]. The two peaks at 574 and 634 cm^{-1} in the higher wavenumber region are attributed to the displacement of the oxygen atom relative to the Mn atom along the octahedral chains since oxygen is 4 times lighter than manganese [65].

Meanwhile, the weak bands at around 295 and 494 cm^{-1} correspond to the phonon density of states instead of allowed zone-centered Raman phonons. This happens because the presence of lattice distortion and crystal defects in the materials confine the phonons [65]. We observe tiny peaks in our pristine MnO_2 sample, and these peaks do not undergo significant changes up to 5% NiO incorporation. Further increase in NiO concentration (7%) strengthened the peak at 295 cm^{-1}. This result demonstrates that this amount of NiO incorporation has enhanced the confinement of phonons by creating more lattice distortion and crystal defects, which agrees well with our SEM and XRD results.

Furthermore, with the incorporation of NiO, variation of peak strength and broadening have been observed for the Raman active peaks at around 346, 574, and 634 cm^{-1} with a tiny shift to the lower frequency. The peak strengthening and broadening occurred for 7% NiO incorporated MnO_2 NWs is higher. These results clearly indicate the distortion of structural lattice parameters, which matches our XRD data. Similar contorted and structural rearrangements of lattice have been reported in Fe-doped MnO_2 composite materials due to oxygen displacement and vacancies [65].

From the above Raman analysis, it is evident that the cooperative interaction between the incorporated 7% NiO and MnO_2 is larger, which can provide lattice distortion and defects involving oxygen displacement and vacancies without structural phase transition. So,

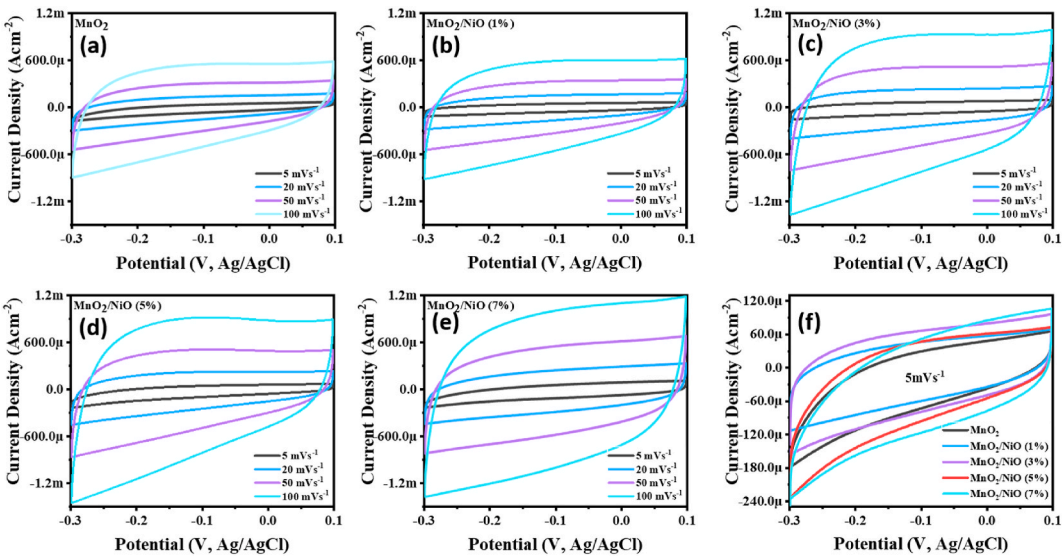

Fig. 6. Cyclic voltammetry curve of (a) MnO_2, (b) MnO_2/NiO (1%), (c) MnO_2/NiO (3%), (d) MnO_2/NiO (5%), MnO_2/NiO (7%), and (f) All samples CV curve at common scan rate 5 mVs^{-1}.

it is expected that the 7%NiO incorporated composite materials can provide better results in ion exchange reactions and improved electrochemical performance.

3.5. Electrochemical properties

Based on charge accumulation and/or storage process, the supercapacitive behavior of MnO_2 can be explained via two mechanisms. One is the rapid adsorption and desorption of electrolyte cations (Na^+) at the interface of the electrode/electrolytes, thus forming an electrically double-layer type capacitor (EDLC) into which the possible reaction mechanism is [66]

$$(MnO_2)_{surface} + Na^+ + e^- \leftrightarrow \left(MnO_2^- Na^+\right)_{surface}.$$

The other mechanism, named pseudocapacitance, is the intercalation of electrolyte cations (Na^+) in the bulk of the electrode materials upon reduction and then followed by deintercalation upon oxidation in the following way [67]:

$$MnO_2 + Na^+ + e^- \leftrightarrow MnOONa.$$

In both of these processes, a redox reaction takes place between the oxidation states of manganese. In the former case, the process is non-faradic, while the latter one undergoes a faradaic process.

3.5.1. Cyclic voltammetry

The faradaic and non-faradic charge storage mechanisms in the prepared MnO_2/NiO composite electrodes have been investigated by cyclic voltammetry (CV) measurements in a three-electrode system with 0.5 M Na_2SO_4 as the electrolyte solution. Fig. 6(a–e) represent the CV profile of the studied composites at various scan rate (5, 20, 50, and 100 mV/s) in the potential range −0.3 V to +0.1 V. Fig. 6(a–e) illustrate the quasi-rectangular CV profile of the all examined materials which indicates that the charge storage mechanism in these active materials is mainly pseudocapacitive in nature [68]. It has been noticed that with the increasing scan rate, the peak current intensity and the enclosed area of the CV curve increase. These overall results illustrate better intercalation/deintercalation of electrolytes and faster faradaic redox reaction kinetics of electrons and ions in the active materials [69]. Furthermore, it is worth observing that at any particular scan rate (*e.g.* 5 mV/s), the area of the CV curve is higher for the 7% NiO incorporated MnO_2 NWs sample compared to other composites, but retaining the shape of the CV profile (Fig. 6(f)). This suggests that this particular concentration of NiO has improved the charge storage in the electrode by providing better connection between the electrochemically active materials and electrolytes and thereby facilitating faster diffusion paths for ion and electron transportation.

3.5.2. Galvanostatic charging-discharging

Since the galvanostatic charging-discharging (GCD) study can provide a quantitative understanding of the supercapacitive properties of electrode materials, the GCD was carried out for all prepared materials at different current densities (1.25, 1.75, and 2.25 A/g), which are presented in Fig. 7(a–e). It is observed that the GCD curve deviated from the ideal symmetric triangular shape for pristine MnO_2 and composite materials due to the reversible conversion reaction. This confirms the pseudocapacitive charge storage behavior of the prepared electrodes and is in agreement with the CV analysis. Also, with increasing the current density, the discharge time was

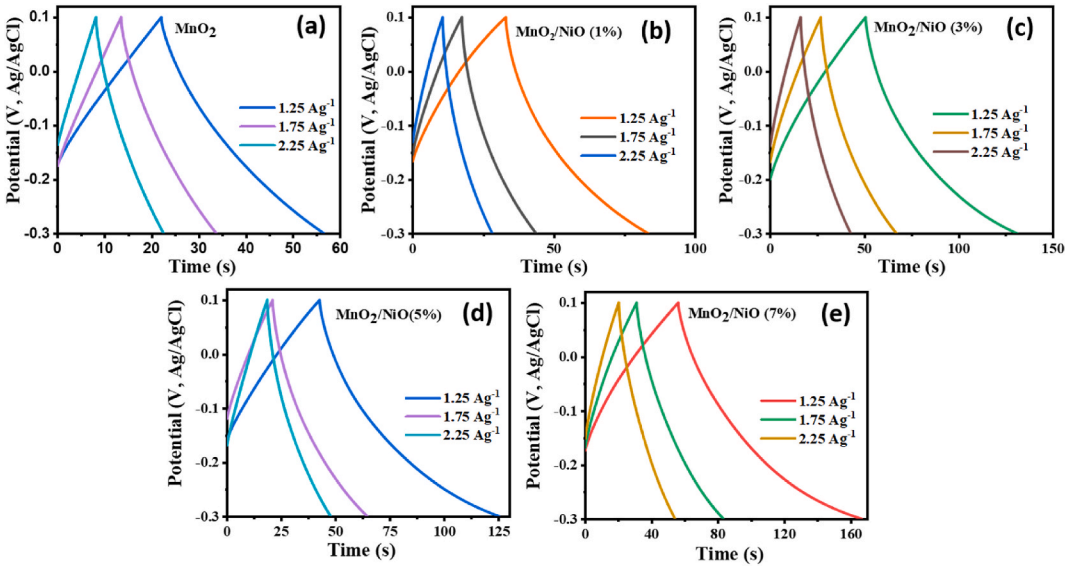

Fig. 7. At different current density, the GCD curves of (a) MnO_2, (b) MnO_2/NiO (1%), (c) MnO_2/NiO (3%), (d) MnO_2/NiO (5%), and (e) MnO_2/NiO (7%) nanocomposites.

found to decrease. This is attributed to the insufficient time for the redox reaction to occur via the diffusion of ions into the inner active sites of the materials [70].

The GCD curves at 1.25 A/g current density have been used to estimate the specific capacitance (C_s) of the fabricated pristine MnO_2 and MnO_2/NiO composites by using the following formula [15] and tabulated in Table 1:

$$C_s = \frac{I \times \Delta t}{m \times \Delta V}.$$

Here, (I/m) is the current density, Δt and ΔV are the discharging time and potential difference, respectively. From the measured value of the specific capacitance, it is elucidated that the highest specific capacitance (343 F/g at a current density of 1.25 A/g) has been achieved in MnO_2/NiO (7%) nanocomposite materials. Using the GCD curve, the MnO_2/NiO (7%) nanocomposite estimated energy density of 7.62 Wh/kg with a power density of 249 W/kg. The higher value of C_s in MnO_2/NiO (7%) composite electrodes may be attributed to the synergistic effect between different morphologically and electrically conducting metal oxides MnO_2 and NiO. In particular, the higher electrically conductive NiO nanoparticles were well attached on MnO_2 nanowires in MnO_2/NiO (7%) composite, which provides larger surface area along with more active sites, enhanced electrically conductive channels and shorter diffusion paths for the efficient and faster migration of electrolyte ions and electrons to the active sites of the electrode. It is worth mentioning that increasing the current density lowered the specific capacitance, which is common in metal oxide-based supercapacitors. This is because, at lower current density, the efficient diffusion of electrolytes occurs through almost every available channel and pores of the active materials, which offers a complete redox reaction. At higher current density, the ions can not penetrate the innermost portion of the active materials and are found in limited accessible areas for diffusion, which diminishes the specific capacitance [71].

3.5.3. Electrochemical impedance spectroscopy (EIS)

The charge transfer ability of MnO_2 is enhanced by compositing with NiO, which can be convinced in Electrochemical impedance spectroscopy (EIS) measurement. EIS is performed at open circuit potential with a 10 mV ac perturbation in the 0.1Hz–100 KHz band. The Nyquist plots of all the synthesized samples are shown in Fig. 8, and the inset of this figure displays a magnified plot for a higher frequency area. The figures show a semicircle at high frequencies and a nearly linear change at low frequencies. The semicircle demonstrates typical charge transfer at the electrode interface [72]. As seen in the inset in Fig. 8, which is the expanded portion at high frequency, the semicircle diameter of the MnO_2/NiO (7%) looked to be significantly smaller, indicating a reduction in the charge-transfer resistance of the MnO_2/NiO (7%) than all the synthesized samples. The electrolytic ion transfer resistance and diffusion from the electrolyte to the surface of the electrode is reflected by the straight sloping line in the low-frequency area. Less diffusion and a higher capacitance of the electrode materials are indicated by a larger slope [73,74]. The slope of MnO_2/NiO nanocomposites is higher than pure α-MnO_2, suggesting that MnO_2/NiO nanocomposites have a lower diffusion resistance and that ion diffusion mass transfer is effective [75]. The EIS data is fitted using an equivalent circuit model made up of bulk solution resistance R_s, charge-transfer resistance R_{ct}, Warburg resistance W_o, and constant phase element *CPE* [76]. The values are shown in Table 2. R_{ct} of samples reveals the characteristics with regard to redox reactions at the electrode/electrolyte interface. Small Rct values often indicate that the charge transfer process may proceed more rapidly and readily due to the reduced resistance characteristics of the electrodes [72]. The R_{ct} value (3 Ω) of the MnO_2/NiO (7%) electrode is the lowest, providing faster charge transfer. Warburg resistance shows the diffusion of ions across the contact of electrolyte and electrode [77]. MnO_2/NiO (7%) nanocomposite has the smallest Warburg resistance among the samples, indicating faster ionic diffusion between active material and electrolyte. Overall, according to the data obtained from the EIS, the MnO_2/NiO (7%) nanocomposite electrode outperforms the other electrodes regarding supercapacitor performance, which is consistent with the findings of the CV and GCD tests.

3.5.4. Cyclic stability

The electrochemical stability of the sample (MnO_2/NiO (7%)) with the highest value of specific capacitance has been studied for 3000 charging-discharging cycles and is shown in Fig. 9. It was observed that the specific capacitance decreased gradually, and a retention of 83% of the initial capacitance after 3000 charging and discharging cycle. For the first 1500 cycles, capacitance gradually decreases, and then it provides a stable value. This stable cyclic stability of MnO_2/NiO may be attributed to the unique structure of the nanocomposite and an improvement in the rate of diffusion of the ions at the interface. The cyclic stability was also studied for the MnO_2 electrodes and a retention of 78% of the initial capacitance after 3000 charging and discharging cycle was obtained. This suggest that the incorporation of NiO nanoparticles enhances the stability of the nanocomposites.

Table 1
The estimated specific capacitance (C_s), energy density (E^d) and power density (p) of MnO_2 and MnO_2/NiO electrodes at constant current density 1.25 A/g in 0.5 M Na_2SO_4 electrolytes solution.

Samples	Specific capacitance (F/g)	Energy density (Wh/kg)	Power density (W/kg)
MnO_2	106	2.35	248
MnO_2/NiO (1%)	159	3.53	249
MnO_2/NiO (3%)	253	5.6	248
MnO_2/NiO (5%)	259	5.75	249
MnO_2/NiO (7%)	343	7.62	249

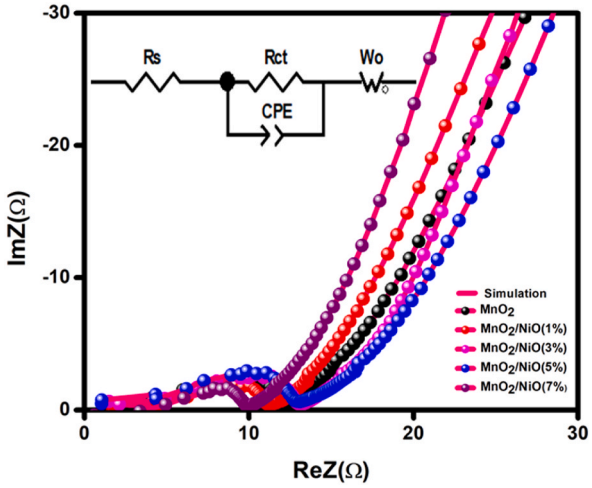

Fig. 8. EIS spectra of MnO_2 and MnO_2/NiO nanocomposites.

Table 2
The equivalent circuit parameters value of MnO_2 nanowires and MnO_2/NiO nanocomposites.

Sample	$R_s(\Omega)$	$R_{ct}(\Omega)$	W_o-$R(\Omega)$
MnO_2	6.81	5.0	7.50
MnO_2/NiO (1%)	7.03	4.0	6.50
MnO_2/NiO (3%)	7.30	5.6	9.50
MnO_2/NiO (5%)	6.30	6.3	11.50
MnO_2/NiO (7%)	6.63	3.0	6.41

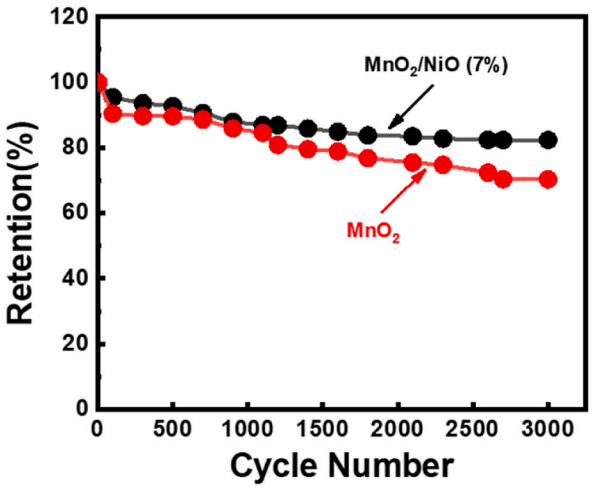

Fig. 9. Cyclic stability for MnO_2 and MnO_2/NiO (7%) nanocomposite for 3000 cycle of operation.

4. Conclusions

In summary, a facile and cost-effective methodology has been employed to fabricate MnO_2/NiO nanocomposites with various concentrations of NiO nanoparticles (0, 1, 3, 5, and 7%). The nanowires-like structure of the as-prepared MnO_2 and MnO_2/NiO nanocomposites has been confirmed by SEM. The structural and compositional studies were performed via XRD, TEM, and Raman which provide substantial information about the synthesized composite materials. The electrochemical behavior of these nanocomposites was then investigated to assess their potential application as electrode materials in supercapacitors. The MnO_2/NiO (7%) nanocomposite delivers better electrochemical performance compared to pristine MnO_2 and other NiO-incorporated MnO_2 composite materials, which achieve maximum specific capacitance (343 F/g) at 1.25 A/g, with good energy 7.62 Wh/kg and power density 249

W/kg. We believe that the synergistic effect between different morphological and electrically conducting MnO_2 and NiO nanomaterials is responsible for the improved electrochemical behavior of these MnO_2/NiO (7%) electrode materials and can be a promising candidate in energy storage devices for the future energy crisis.

Data availability statement

Data will be made available on request.

CRediT authorship contribution statement

Muhammad Rakibul Islam: Writing – review & editing, Writing – original draft, Supervision, Resources, Project administration, Methodology, Investigation, Funding acquisition, Formal analysis, Conceptualization. **Mahabub Alam Bhuiyan:** Writing – review & editing, Writing – original draft, Methodology, Formal analysis. **Md Hasive Ahmed:** Writing – review & editing, Methodology, Investigation, Data curation. **Mizanur Rahaman:** Writing – review & editing, Investigation, Formal analysis, Data curation.

Declaration of competing interest

The authors declare that they have no known competing financial interests or personal relationships that could have appeared to influence the work reported in this paper.

Acknowledgments

The authors gratefully acknowledge the financial support from the Ministry of Science and Technology, Government of Bangladesh, under grant 39.00.0000.009.99.023.23–363 (Project ID# SRG-236627).

Appendix A. Supplementary data

Supplementary data to this article can be found online at https://doi.org/10.1016/j.heliyon.2024.e26631.

References

[1] K. Sharma, A. Arora, S.K. Tripathi, Review of supercapacitors: materials and devices, J. Energy Storage 21 (2019) 801–825.
[2] X. He, X. Zhang, A comprehensive review of supercapacitors: properties, electrodes, electrolytes and thermal management systems based on phase change materials, J. Energy Storage 56 (2022) 106023.
[3] M. Kandasamy, A. Seetharaman, B. Chakraborty, I.M. Babu, J.J. William, G. Muralidharan, K. Jothivenkatachalam, D. Sivasubramanian, Experimental and theoretical investigation of the energy-storage behavior of a polyaniline-linked reduced-graphene-oxide–Sn O 2 ternary nanohybrid electrode, Phys. Rev. Appl. 14 (2) (2020) 024067.
[4] S. Chu, Y. Cui, N. Liu, The path towards sustainable energy, Nat. Mater. 16 (1) (2017) 16–22.
[5] M.H. Ahmad, R.B. Alam, A. Ul-Hamid, S.F.U. Farhad, M.R. Islam, Hydrothermal synthesis of Co_3O_4 nanoparticles decorated three dimensional MoS_2 nanoflower for exceptionally stable supercapacitor electrode with improved capacitive performance, J. Energy Storage 47 (2022) 103551.
[6] A. Muzaffar, M.B. Ahamed, K. Deshmukh, J. Thirumalai, A review on recent advances in hybrid supercapacitors: design, fabrication and applications, Renew. Sustain. Energy Rev. 101 (2019) 123–145.
[7] B. Varshney, M.J. Siddiqui, A.H. Anwer, M.Z. Khan, F. Ahmed, A. Aljaafari, H.H. Hammud, A. Azam, Synthesis of mesoporous SnO_2/NiO nanocomposite using modified sol–gel method and its electrochemical performance as electrode material for supercapacitors, Sci. Rep. 10 (1) (2020) 11032.
[8] J. Chen, J. Xu, S. Zhou, N. Zhao, C.P. Wong, Nitrogen-doped hierarchically porous carbon foam: a free-standing electrode and mechanical support for high-performance supercapacitors, Nano Energy 25 (2016) 193–202.
[9] T.S. Mathis, N. Kurra, X. Wang, D. Pinto, P. Simon, Y. Gogotsi, Energy storage data reporting in perspective—guidelines for interpreting the performance of electrochemical energy storage systems, Adv. Energy Mater. 9 (39) (2019) 1902007 s.
[10] L. Kong, C. Tang, H.J. Peng, J.Q. Huang, Q. Zhang, Advanced energy materials for flexible batteries in energy storage: a review, SmartMat 1 (1) (2020).
[11] K. Silambarasan, J. Joseph, Flexible anion microbatteries: towards construction of a hybrid battery–capacitor device, ChemSusChem 11 (18) (2018) 3081–3086.
[12] J. Yan, Q. Wang, T. Wei, Z. Fan, Recent advances in design and fabrication of electrochemical supercapacitors with high energy densities, Adv. Energy Mater. 4 (4) (2014) 1300816.
[13] A. Dang, T. Li, C. Xiong, T. Zhao, Y. Shang, H. Liu, X. Chen, H. Li, Q. Zhuang, S. Zhang, Long-life electrochemical supercapacitor based on a novel hierarchically carbon foam templated carbon nanotube electrode, Compos. B Eng. 141 (2018) 250–257.
[14] J. Lim, G.Y. Lee, H.J. Lee, S.K. Cha, D.S. Choi, S.H. Koo, W.J. Lee, S.O. Kim, Open porous graphene nanoribbon hydrogel via additive-free interfacial self-assembly: fast mass transport electrodes for high-performance biosensing and energy storage, Energy Storage Mater. 16 (2019) 251–258.
[15] Z.M. Riyas, C. Priya, R. Premila, G. Maheshwaran, S. Sudhahar, M.R. Prabhu, Synergistic effect of La_2O_3-NiO nanocomposite based electrode for electrochemical high-performance asymmetric supercapacitor applications, J. Energy Storage 53 (2022) 104988.
[16] S. Suganya, G. Maheshwaran, M.R. Prabhu, P. Devendran, M.K. Kumar, S. Sudhahar, Enhanced electrochemical activity of ternary Co-Mn-Zn oxide for the fabrication of hybrid supercapacitor applications, J. Energy Storage 56 (2022) 106057.
[17] M. Girirajan, V. Arumugam, S. Subramaniyan, R.P. Manimuthu, S. Sakkarapani, Two-dimensional layered bismuthene/Antimonene nanocomposite as a potential electrode material for the fabrication of high-energy density hybrid supercapacitors, Energy Fuel. 36 (19) (2022) 12299–12309.
[18] S.S. Kv, J. Santo, P.K. Penumakala, Effect of surface modification of printed electrodes on the performance of supercapacitors, J. Energy Storage 56 (2022) 106043.
[19] S. Najib, E. Erdem, Current progress achieved in novel materials for supercapacitor electrodes: mini review, Nanoscale Adv. 1 (8) (2019) 2817–2827.
[20] G. Zhang, X. Xiao, B. Li, P. Gu, H. Xue, H. Pang, Transition metal oxides with one-dimensional/one-dimensional-analogue nanostructures for advanced supercapacitors, J. Mater. Chem. A 5 (18) (2017) 8155–8186.

[21] K. Zhang, X. Han, Z. Hu, X. Zhang, Z. Tao, J. Chen, Nanostructured Mn-based oxides for electrochemical energy storage and conversion, Chem. Soc. Rev. 44 (3) (2015) 699–728.
[22] X. Xia, D. Chao, Z. Fan, C. Guan, X. Cao, H. Zhang, H.J. Fan, A new type of porous graphite foams and their integrated composites with oxide/polymer core/shell nanowires for supercapacitors: structural design, fabrication, and full supercapacitor demonstrations, Nano Lett. 14 (3) (2014) 1651–1658.
[23] M. Zhu, Y. Wang, D. Meng, X. Qin, G. Diao, Hydrothermal synthesis of hematite nanoparticles and their electrochemical properties, J. Phys. Chem. C 116 (30) (2012) 16276–16285.
[24] S. Vijayakumar, S. Nagamuthu, G. Muralidharan, Supercapacitor studies on NiO nanoflakes synthesized through a microwave route, ACS Appl. Mater. Interfaces 5 (6) (2013) 2188–2196.
[25] A. Kumar, A. Sanger, A. Kumar, Y. Kumar, R. Chandra, An efficient α-MnO_2 nanorods forests electrode for electrochemical capacitors with neutral aqueous electrolytes, Electrochim. Acta 220 (2016) 712–720.
[26] M. Toupin, T. Brousse, D. Bélanger, Charge storage mechanism of MnO_2 electrode used in aqueous electrochemical capacitor, Chem. Mater. 16 (16) (2004) 3184–3190.
[27] J.K. Chang, W.T. Tsai, Material characterization and electrochemical performance of hydrous manganese oxide electrodes for use in electrochemical pseudocapacitors, J. Electrochem. Soc. 150 (10) (2003) A1333.
[28] Y. Gogotsi, P. Simon, True performance metrics in electrochemical energy storage, Science 334 (6058) (2011) 917–918.
[29] X. Lang, A. Hirata, T. Fujita, M. Chen, Nanoporous metal/oxide hybrid electrodes for electrochemical supercapacitors, Nat. Nanotechnol. 6 (4) (2011) 232–236.
[30] W. Li, K. Xu, B. Li, J. Sun, F. Jiang, Z. Yu, R. Zou, Z. Chen, J. Hu, MnO_2 nanoflower arrays with high rate capability for flexible supercapacitors, Chemelectrochem 1 (6) (2014) 1003–1008.
[31] P. Yang, Y. Ding, Z. Lin, Z. Chen, Y. Li, P. Qiang, M. Ebrahimi, W. Mai, C.P. Wong, Z.L. Wang, Low-cost high-performance solid-state asymmetric supercapacitors based on MnO_2 nanowires and Fe_2O_3 nanotubes, Nano Lett. 14 (2) (2014) 731–736.
[32] X. Lu, D. Zheng, T. Zhai, Z. Liu, Y. Huang, S. Xie, Y. Tong, Facile synthesis of large-area manganese oxide nanorod arrays as a high-performance electrochemical supercapacitor, Energy Environ. Sci. 4 (8) (2011) 2915–2921.
[33] J.G. Wang, F. Kang, B. Wei, Engineering of MnO_2-based nanocomposites for high-performance supercapacitors, Prog. Mater. Sci. 74 (2015) 51–124.
[34] Q.Z. Zhang, D. Zhang, Z.C. Miao, X.L. Zhang, S.L. Chou, Research progress in MnO2–carbon based supercapacitor electrode materials, Small 14 (24) (2018) 1702883.
[35] P. Sen, A. De, A.D. Chowdhury, S.K. Bandyopadhyay, N. Agnihotri, M. Mukherjee, Conducting polymer based manganese dioxide nanocomposite as supercapacitor, Electrochim. Acta 108 (2013) 265–273.
[36] M. Huang, Y. Zhang, F. Li, Z. Wang, Alamusi, N. Hu, Z. Wen, Q. Liu, Merging of Kirkendall growth and Ostwald ripening: CuO@MnO_2 core-shell architectures for asymmetric supercapacitors, Sci. Rep. 4 (1) (2014) 4518.
[37] J. Shao, X. Zhou, Q. Liu, R. Zou, W. Li, J. Yang, J. Hu, Mechanism analysis of the capacitance contributions and ultralong cycling-stability of the isomorphous MnO_2@MnO_2 core/shell nanostructures for supercapacitors, J. Mater. Chem. A 3 (11) (2015) 6168–6176.
[38] R.S. Kate, S.A. Khalate, R.J. Deokate, Overview of nanostructured metal oxides and pure nickel oxide (NiO) electrodes for supercapacitors: a review, J. Alloys Compd. 734 (2018) 89–111.
[39] W. Deng, Y. Liu, Y. Zhang, F. Lu, Q. Chen, X. Ji, Enhanced electrochemical capacitance of nanoporous NiO based on an eggshell membrane, RSC Adv. 2 (5) (2012) 1743–1745.
[40] C. Yuan, X. Zhang, L. Su, B. Gao, L. Shen, Facile synthesis and self-assembly of hierarchical porous NiO nano/micro spherical superstructures for high performance supercapacitors, J. Mater. Chem. 19 (32) (2009) 5772–5777.
[41] Y. Qian, R. Liu, Q. Wang, J. Xu, D. Chen, G. Shen, Efficient synthesis of hierarchical NiO nanosheets for high-performance flexible all-solid-state supercapacitors, J. Mater. Chem. A 2 (28) (2014) 10917–10922.
[42] J. Liu, J. Jiang, M. Bosman, H.J. Fan, Three-dimensional tubular arrays of MnO_2–NiO nanoflakes with high areal pseudocapacitance, J. Mater. Chem. 22 (6) (2012) 2419–2426.
[43] Y. Li, H. Peng, C. Zhang, M. Chu, P. Xiao, Y. Zhang, Branched ultra-fine nickel oxide/manganese dioxide core–shell nanosheet arrays for electrochemical capacitors, RSC Adv. 5 (94) (2015) 77115–77121.
[44] M. AlAnazi, T. Ghrib, F. Ercan, M. Alsubaie, T. Demirci, Ö. Kaygili, T.S. Kayed, I. Ercan, Structural, Optical, and Electrical Investigation of Multilayered MnO_2 (n)/NiO (P) Heterojunctions for Supercapacitors Applications, Surfaces and Interfaces, 2023 103321.
[45] X. Zhao, X. Liu, F. Li, M. Huang, MnO_2@ NiO nanosheets@ nanowires hierarchical structures with enhanced supercapacitive properties, J. Mater. Sci. 55 (6) (2020) 2482–2491.
[46] N. Zhang, G. Guo, B. He, J. Zhu, J. Wu, J. Qiu, Synthesis and research of MnO_2–NiO composite as lithium-ion battery anode using spent Zn–Mn batteries as manganese source, J. Alloys Compd. 838 (2020) 155578.
[47] M. Arunpandian, K. Selvakumar, E.R. Nagarajan, T.H. Oh, Evaluation of rGO decorated MnO_2/NiO nanocomposite for high-performance photocatalytic and supercapacitor applications, Diam. Relat. Mater. 139 (2023) 110383.
[48] Y. Bi, A. Nautiyal, H. Zhang, J. Luo, X. Zhang, One-pot microwave synthesis of NiO/MnO_2 composite as a high-performance electrode material for supercapacitors, Electrochim. Acta 260 (2018) 952–958.
[49] T.F. Yi, J. Mei, B. Guan, P. Cui, S. Luo, Y. Xie, Y. Liu, Construction of spherical NiO@MnO_2 with core-shell structure obtained by depositing MnO_2 nanoparticles on NiO nanosheets for high-performance supercapacitor, Ceram. Int. 46 (1) (2020) 421–429.
[50] K.M. Racik, K. Guruprasad, M. Mahendiran, J. Madhavan, T. Maiyalagan, M.V.A. Raj, Enhanced electrochemical performance of MnO_2/NiO nanocomposite for supercapacitor electrode with excellent cycling stability, J. Mater. Sci. Mater. Electron. 30 (2019) 5222–5232.
[51] M. Zhang, X. Dai, C. Zhang, Y. Fuan, D. Yang, J. Li, High specific capacitance of the electrodeposited MnO_2 on porous foam nickel soaked in alcohol and its dependence on precursor concentration, Materials 13 (1) (2020) 181.
[52] D.P. Dubal, D. Aradilla, G. Bidan, P. Gentile, T.J. Schubert, J. Wimberg, S. Sadki, P. Gomez-Romero, 3D hierarchical assembly of ultrathin MnO_2 nanoflakes on silicon nanowires for high performance micro-supercapacitors in Li-doped ionic liquid, Sci. Rep. 5 (1) (2015) 9771.
[53] R. Wang, X. Yan, Superior asymmetric supercapacitor based on Ni-Co oxide nanosheets and carbon nanorods, Sci. Rep. 4 (1) (2014) 3712.
[54] R. Zou, M.F. Yuen, Z. Zhang, J. Hu, W. Zhang, Three-dimensional networked $NiCo_2O_4$/MnO_2 branched nanowire heterostructure arrays on nickel foam with enhanced supercapacitor performance, J. Mater. Chem. A 3 (4) (2015) 1717–1723.
[55] S.D. Dhas, P.S. Maldar, M.D. Patil, A.B. Nagare, M.R. Waikar, R.G. Sonkawade, A.V. Moholkar, Synthesis of NiO nanoparticles for supercapacitor application as an efficient electrode material, Vacuum 181 (2020) 109646.
[56] J. Chen, Y. Wang, X. He, S. Xu, M. Fang, X. Zhao, Y. Shang, Electrochemical properties of MnO_2 nanorods as anode materials for lithium ion batteries, Electrochim. Acta 142 (2014) 152–156.
[57] Y. Duan, Z. Liu, Y. Zhang, M. Wen, A theoretical study of the dielectric and magnetic responses of Fe-doped α-MnO_2 based on quantum mechanical calculations, J. Mater. Chem. C 1 (10) (2013) 1990–1994.
[58] M. Lubke, A. Sumboja, L. McCafferty, C.F. Armer, A.D. Handoko, Y. Du, K. McColl, F. Cora, D. Brett, Z. Liu, J.A. Darr, Transition-metal-doped alpha-MnO_2 nanorods as bifunctional catalysts for efficient oxygen reduction and evolution reactions, ChemistrySelect 3 (9) (2018) 2613–2622.
[59] V. Radmilovic, H.A. Gasteiger, P.N. Ross, Structure and chemical composition of a supported Pt-Ru electrocatalyst for methanol oxidation, J. Catal. 154 (1) (1995) 98–106.
[60] W.S. Hummers Jr., R.E. Offeman, Preparation of graphitic oxide, J. Am. Chem. Soc. 80 (6) (1958), 1339-1339.
[61] C. Kittle, Introduction to Solid State Physics, eighth ed., John Wiley and Sons, Inc.
[62] T. Gao, M. Glerup, F. Krumeich, R. Nesper, H. Fjellvåg, P. Norby, Microstructures and spectroscopic properties of cryptomelane-type manganese dioxide nanofibers, J. Phys. Chem. C 112 (34) (2008) 13134–13140.

[63] Y. Wang, H. Guan, S. Du, Y. Wang, A facile hydrothermal synthesis of MnO_2 nanorod–reduced graphene oxide nanocomposites possessing excellent microwave absorption properties, RSC Adv. 5 (108) (2015) 88979–88988.
[64] S. Jana, S. Pande, A.K. Sinha, S. Sarkar, M. Pradhan, M. Basu, S. Saha, T. Pal, A green chemistry approach for the synthesis of flower-like Ag-doped MnO_2 nanostructures probed by surface-enhanced Raman spectroscopy, J. Phys. Chem. C 113 (4) (2009) 1386–1392.
[65] E. Hastuti, A. Subhan, P. Amonpattaratkit, M. Zainuri, S. Suasmoro, The effects of Fe-doping on MnO_2: phase transitions, defect structures and its influence on electrical properties, RSC Adv. 11 (14) (2021) 7808–7823.
[66] S.C. Pang, M.A. Anderson, T.W. Chapman, Novel electrode materials for thin-film ultracapacitors: comparison of electrochemical properties of sol-gel-derived and electrodeposited manganese dioxide, J. Electrochem. Soc. 147 (2) (2000) 444.
[67] H.Y. Lee, J.B. Goodenough, Supercapacitor behavior with KCl electrolyte, J. Solid State Chem. 144 (1) (1999) 220–223.
[68] S. Fleischmann, J.B. Mitchell, R. Wang, C. Zhan, D.E. Jiang, V. Presser, V. Augustyn, Pseudocapacitance: from fundamental understanding to high power energy storage materials, Chem. Rev. 120 (14) (2020) 6738–6782.
[69] J.H. Kim, K. Zhu, Y. Yan, C.L. Perkins, A.J. Frank, Microstructure and pseudocapacitive properties of electrodes constructed of oriented NiO-TiO_2 nanotube arrays, Nano Lett. 10 (10) (2010) 4099–4104.
[70] S. Alkhalaf, C.K. Ranaweera, P.K. Kahol, K. Siam, H. Adhikari, S.R. Mishra, F. Perez, B.K. Gupta, K. Ramasamy, R.K. Gupta, Electrochemical energy storage performance of electrospun $CoMn_2O_4$ nanofibers, J. Alloys Compd. 692 (2017) 59–66.
[71] D. Sarkar, G.G. Khan, A.K. Singh, K. Mandal, High-performance pseudocapacitor electrodes based on α-Fe_2O_3/MnO_2 core–shell nanowire heterostructure arrays, J. Phys. Chem. C 117 (30) (2013) 15523–15531.
[72] Y. Li, J. Li, H. Xie, F. Yang, Y. Zhou, Structural and electrochemical performances of α-MnO_2 doped with tin for supercapacitors, J. Wuhan Univ. Technol.-Materials Sci. Ed. 32 (2) (2017) 237–244.
[73] Rusi, S.R. Majid, Effects of electrodeposition mode and deposition cycle on the electrochemical performance of MnO_2-NiO composite electrodes for high-energy-density supercapacitors, PLoS One 11 (5) (2016) e0154566.
[74] M.D. Stoller, S. Park, Y. Zhu, J. An, R.S. Ruoff, Graphene-based ultracapacitors, Nano Lett. 8 (10) (2008) 3498–3502.
[75] H. Lin, M. Zhang, J. Miao, L. Li, K. Xin, X. Liao, Z. Feng, Synthesis and electrochemical properties of Er/α-MnO_2 microspheres for supercapacitors application, Ionics 25 (2019) 3867–3873.
[76] A.V. Radhamani, K.M. Shareef, M.R. Rao, ZnO@MnO_2 core–shell nanofiber cathodes for high performance asymmetric supercapacitors, ACS Appl. Mater. Interfaces 8 (44) (2016) 30531–30542.
[77] C. Portet, P.L. Taberna, P. Simon, C. Laberty-Robert, Modification of Al current collector surface by sol–gel deposit for carbon–carbon supercapacitor applications, Electrochim. Acta 49 (6) (2004) 90.